





# Advanced Digital Signal Processing and Variable-Rate Coding for Unrepeated Optical Transmission

José Hélio C. Júnior , Tiago Sutili , Rafael C. Figueiredo , *Member, IEEE*, and Darli A. A. Mello 

**Abstract**—In this paper, we evaluate the selective combination of algorithms for fiber nonlinearity compensation, transceiver impairments mitigation and variable-rate coding in unrepeated optical transmission. A post-emphasis filter and a two-stage  $4 \times 4$  multiple-input and multiple-output equalizer compensate the impact of bandwidth limitations and in-phase and quadrature skew. Nonlinear compensation is accomplished by a fast-converging adaptive digital back-propagation algorithm and maximum likelihood sequence estimation. Forward error correction is provided by a variable-rate spatially-coupled low-density parity-check code. The performance and complexity of the proposed digital subsystems are experimentally evaluated by the unrepeated wavelength division multiplexing transmission of  $17 \times 200$ -Gb/s (DP-16QAM 32-GBd) channels over 350-km of large effective area and low-loss single-mode fibers. The experimental results for different combinations of algorithms elucidate the trade-off of complexity and performance in unrepeated optical transmission.

**Index Terms**—Coherent optical communications, transceiver impairments mitigation, fiber nonlinearity compensation, forward error correction, unrepeated transmission.

## I. INTRODUCTION

UNREPEATED coherent optical transmission, without active elements along the link, is an attractive solution to provide high-capacity connectivity in remote areas, simplifying the system architecture and reducing the solution cost. In unrepeated transmission, the system performance is essentially limited by the trade-off between the nonlinear Kerr effect and amplified spontaneous emission (ASE) noise generated in optical amplifiers. With less impact, eventually, transceiver impairments such as bandwidth limitations and in-phase and quadrature (IQ) skews may also impair the transmission performance. Recently, techniques for nonlinearity compensation have been investigated, and digital back-propagation (DBP) and maximum likelihood sequence estimation (MLSE) arise as

possible solutions [1]. DBP requires the precise estimation of the fiber nonlinear parameter  $\gamma$  for optimum performance. To address this issue, an adaptive DBP (ADBP) has been proposed for tracking the fiber parameters [2]. In addition to nonlinear compensation, variable-rate forward error correction (FEC) [3] is also an essential subsystem for unrepeated optical transmission. As in unrepeated optical links the link length is predetermined, variable-rate coding allows to extract the highest possible data rate. Among several other options for variable-rate coding [4]–[7], spatially-coupled low-density parity-check (SC-LDPC) codes are a promising solution [8].

Several works on nonlinear compensation and FEC schemes for unrepeated optical systems have been reported. Rosa *et al.* present in [9] the single-channel 28 GBd DP-64QAM unrepeated transmission over up to 200 km of single-mode fiber (SMF) employing different Raman amplification schemes and DBP. Wang *et al.* demonstrate in [10] a Nyquist superchannel unrepeated transmission of 447 Gb/s ( $8 \times 55.97$  Gb/s) DP-64QAM over a single span of 160 km of SMF using backward Raman amplification and DBP. We propose in [2] a fast-converging ADBP algorithm based on the gradient descent algorithm with momentum (GDAM). The mean square error (MSE) derived from the dynamic equalizer (DE) is used as cost function (CF). The proposed algorithm is evaluated by the unrepeated transmission of  $17 \times 200$  Gb/s channels (DP-16QAM 32 GBd) over 350 km of large effective area and low loss single-mode fibers (LL-SMF). Januario *et al.* present in [11] a  $10 \times 400$  Gb/s (DP-16QAM 32 GBd) dual-carrier unrepeated transmission over 350 km and 370 km of large effective area and LL-SMF fibers with and without DBP algorithm, respectively, and with SC-LDPC. The same group demonstrate in [12] a  $16 \times 400$  Gb/s (DP-16QAM 66 GBd) unrepeated transmission over 400 km of ultra-low loss and large effective area fibers using SC-LDPC, while in [13] a  $24 \times 400$  Gb/s (DP-16QAM 64/66 GBd) unrepeated transmission over 443.1 km of ultra-low loss and large effective area and LL-SMF fibers employing DBP and SC-LDPC is presented. Although several signal processing and coding techniques for unrepeated transmission have been individually proposed, to the best of our knowledge, an unifying analysis of nonlinearity compensation, transceiver impairments mitigation and coding schemes, and their potential rate gains and complexity analysis, has not been presented.

In this paper, we evaluate a digital receiver combining linear and nonlinear DSP-based distortion mitigation, and

Manuscript received March 29, 2022; revised May 18, 2022; accepted June 9, 2022. Date of publication June 14, 2022; date of current version June 23, 2022. This work was supported by FUNTTEL/Finep, CNPq, and FAPESP under Grants 2015/24341-7 and 2015/24517-8. (Corresponding author: José Hélio C. Júnior.)

José Hélio C. Júnior and Darli A. A. Mello are with the School of Electrical and Computer Engineering, University of Campinas, Campinas 13083-970, Brazil (e-mail: joseheliiodacruzjunior@gmail.com; darli@unicamp.br).

Tiago Sutili and Rafael C. Figueiredo are with the Optical Communication Solutions, CPQD, Campinas 13086-902, Brazil (e-mail: tsutili@cpqd.com.br; rafaelcf@cpqd.com.br).

Digital Object Identifier 10.1109/JPHOT.2022.3182903

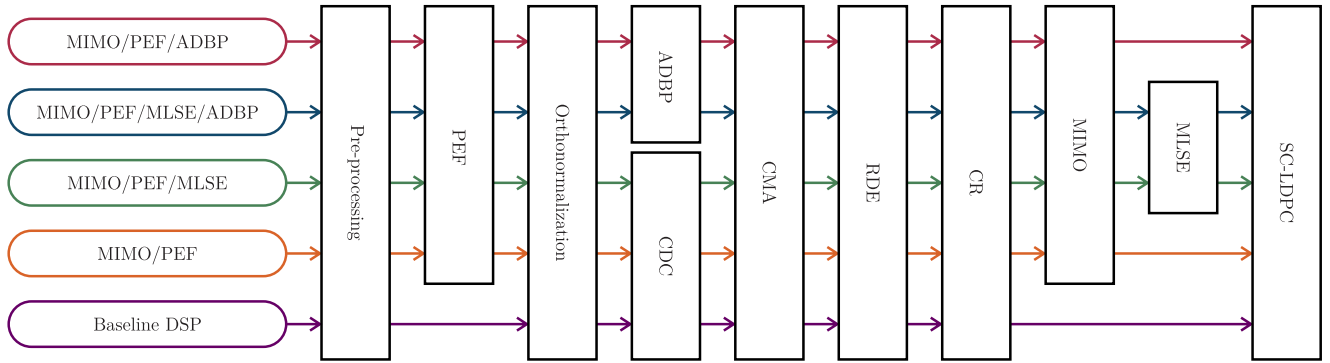


Fig. 1. Block diagram of digital subsystems for the advanced and baseline DSP.

variable-rate FEC. A post-emphasis filter (PEF) and a two-stage  $4 \times 4$  multiple-input and multiple-output (MIMO) equalizer mitigate the impact of bandwidth limitations and IQ skew. A fast-converging ADBP and MLSE are employed for the joint compensation of linear and nonlinear effects. Finally, forward error correction is provided by a variable-rate SC-LDPC code. The digital signal processing (DSP) and coding algorithms are experimentally evaluated in an unrepeated WDM link consisting of transmission of  $17 \times 32$ -GBd DP-16QAM channels over 350-km of large effective area and LL-SMF. We evaluate the computational complexity of linear and nonlinear algorithms using analytic equations. Although the numerical results in this paper are obtained for a specific link setup and modulation format, its framework, including complexity expressions, also apply to more general scenarios.

The remainder of this paper is divided as follows. Section II details the proposed digital receiver. Section III presents the experimental setup. Section IV shows the experimental results. Lastly, Section V concludes the paper.

## II. DIGITAL RECEIVER SUBSYSTEM

The block diagram of the evaluated digital receiver is shown in Fig. 1. The standard DSP (purple line) chain, used here as baseline, considers first the resampling to 2 Sa/Symbol in the pre-processing block<sup>1</sup>. Next, orthonormalization compensates the optical front-end distortions and in-phase and quadrature imbalances using the Gram-Schmidt orthogonalization procedure (GSOP). The following block is chromatic dispersion compensation (CDC) implemented in the frequency domain. Next, dynamic equalization (DE) is carried out by a radius-directed equalizer (RDE) with 15 taps, after constant modulus algorithm (CMA) pre-convergence. Frequency recovery is performed using the  $M$ th power algorithm and phase recovery is accomplished by the blind phase search (BPS) algorithm with 20 test phases, window size of 80, and step size of 40.

Alternatively, the evaluated advanced DSP considers different algorithm combinations. The MIMO/PEF (orange line) adds a post-emphasis filter (PEF) [15] with a 1st-order Gaussian shape

and 35-GHz cutoff frequency, compensating bandwidth limitation imposed by system components. A two-stage  $4 \times 4$  MIMO equalizer [16] is applied for IQ skew mitigation, where the first stage is used for pre-convergence. The MIMO/PEF/ADBP (red line) chain replaces CDC by ADBP for CD and Kerr nonlinearity compensation. The MIMO/PEF/MLSE (green line) and MIMO/PEF/ADBP/MLSE (blue line) chains include MLSE equalization. The short-memory MLSE equalizer accounts for residual intersymbol interference (ISI) left over by previous algorithms in the DSP chain. This ISI can be caused by linear (e.g. narrowband filtering) and nonlinear effects (e.g. self-phase modulation). Specifically in this implementation, soft-output MLSE based on Bahl, Cocke, Jelinek, and Raviv algorithm [17] is performed considering a channel memory equal to 2. As input values, the soft-decision FEC (SD-FEC) decoder requires the log-likelihood ratio (LLR) of each bit. For example, for 16QAM modulation, four LLR values are calculated from one received symbol. Finally, for each DSP implementation, error correction is carried out considering the decoding step as presented in [18]. The soft-decision left-terminated SC-LDPC is generated from protographs [19] with syndrome former memory equal to 2 and decoded with a sliding window of length 15. Specific FEC overhead values are obtained by shortening a mother code [20] with 50000 columns. In addition to codes with variable rates, probabilistic shaping (PS) has been also extensively studied to adapt the data rate [21], [22]. PS requires a well-designed distribution matcher [23] and optimized signal processing algorithms to avoid losses in equalization [24], clock recovery [25] and phase recovery [26]. Therefore, although not exhausting all solutions for rate adaptation, the variable-rate FEC investigated in this paper is a viable solution.

## III. EXPERIMENTAL SETUP

The experimental setup used to evaluate the proposed digital receiver is shown in Fig. 2. At the transmitter, a complete conventional DSP stack is employed. First, a binary sequence is generated and mapped into constellation symbols (16QAM), which are upsampled and filtered by a root-raised-cosine filter (0.1 roll-off factor). The digital-to-analog converter (DAC), operating at 64 GSa/s with 8-bit resolution, converts the signal to the analog domain with a symbol rate equal to 32 GBd, yielding

<sup>1</sup>Although DAC sampling rates are usually lower than 2 Sa/Symbol, it is a common practice to resample the signal to 2 Sa/Symbol at the beginning of the DSP chain [14].

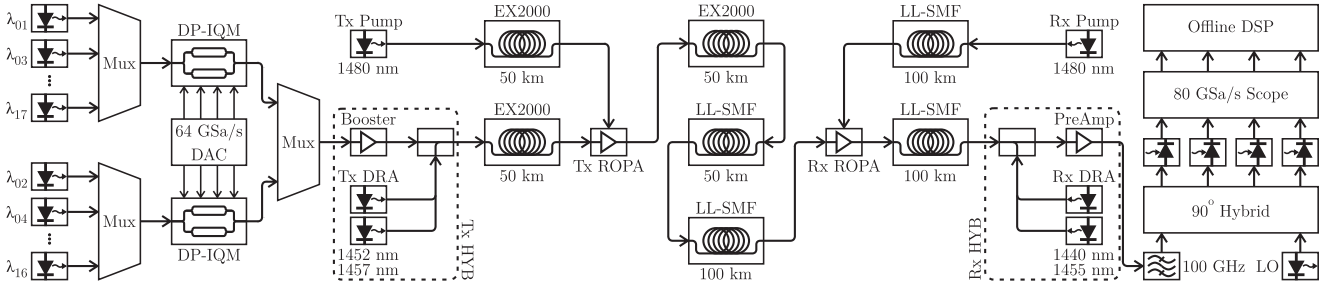


Fig. 2. Experimental setup for unrepeated transmission of  $17 \times 32$ -GBd DP-16QAM channels.

256 Gb/s 16QAM considering I/Q modulation and polarization multiplexing. The four positive DAC outputs drive a LiNbO<sub>3</sub> dual-polarization quadrature modulator (DP-IQM), while the four negative outputs drive a second DP-IQM, modulating 17 channels separated by two arrays of 50-GHz-spaced (from 1552.93 nm up to 1559.39 nm) external cavity lasers (ECL) (100-kHz linewidth). Finally, odd and even carriers are separately modulated by the two DP-IQMs coupled for wavelength-multiplexed transmission.

The unrepeated optical link consists of five fiber segments for signal transmission, and two dedicated fibers for remote pumps. The first segment starts at the transmitter side with a hybrid amplifier (Tx HYB), encompassing an erbium-doped fiber amplifier (EDFA) booster combined with distributed Raman amplification (DRA). The WDM signal is transmitted along with the Raman pumps, which provide 300 mW total power, shared between two pump lasers with wavelengths at 1452 nm and 1457 nm. Next, after 50 km of EX2000 large effective area ultra-low loss fiber (112- $\mu\text{m}^2$  effective area and 0.157-dB/km attenuation), a remote optically pumped amplifier (Tx ROPA) is energized by a 1480-nm pump delivered by a dedicated fiber. The ROPA is followed by a 200-km fiber link consisting of 50 km of EX2000 fiber, and 150 km of LL-SMF (82- $\mu\text{m}^2$  effective area and 0.18-dB/km attenuation). The receiver-side remote amplifier (Rx ROPA) uses 100-km of dedicated LL-SMF to propagate its 1480-nm pump signal. We employed submarine-grade Corning Vascade EX2000 for the first two segments to reduce the nonlinear effects. In the first two fiber segments, the optical channels are launched with the same power. We switch to the more cost-effective LL-SMF in the last three segments, where the signal power is lower, as depicted by the simulated power map in Fig. 3. The Tx and Rx ROPAs consider a launch power into dedicated pump fibers of 1.5 W and 700 mW, respectively. The erbium-doped fiber (EDF) lengths for the Tx/Rx ROPAs were previously optimized resulting, respectively, in 5 m and 9 m, and being positioned at 50 km and 100 km from the respective terminals. The ROPAs are designed based on the optimization procedure proposed in [27].

Finally, the receiver uses a second hybrid amplifier (Rx HYB), encompassing an EDFA pre-amplifier combined with a second counter-propagating DRA. The received WDM signal is transmitted along with the Raman pumps, which provide 500 mW total power, shared between two pump lasers with wavelengths at

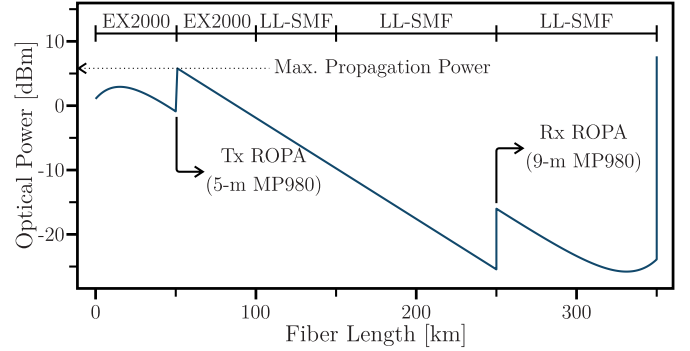


Fig. 3. Simulated power profile.

1440 nm and 1455 nm. After propagation, the central channel is filtered and detected by a polarization-diversity coherent optical receiver. The discrete-component receiver included a 90° optical hybrid connected to a 16-dBm local oscillator with 100-kHz linewidth. The four optical outputs are converted to the electrical domain using 40-GHz balanced photodetectors (PD). Finally, the four electrical signals are sampled at 80 GSa/s by a 4-channel real-time oscilloscope for offline processing using the block diagram presented in Fig. 1.

## IV. EXPERIMENTAL RESULTS

### A. ADBP and $4 \times 4$ MIMO Optimization

We first optimize the number of steps per span considered on the ADBP algorithm. We maximize the  $Q^2$  factor for the central channel considering a constant 1-dBm launch power. The ADBP steps are uniformly distributed along the first three fiber spans, while, aiming to reduce the computational cost, only linear equalization is applied in the last two fibers. The Fig. 4 indicates that the  $Q^2$  factor is optimized for a number of steps per span equal to 12. We next optimize the number of filter taps and step size used in the two-stage  $4 \times 4$  MIMO equalizer. The results are shown in Fig. 5 for the central channel. As expected, increasing the number of taps and decreasing the convergence factor improves the performance of the two-stage  $4 \times 4$  MIMO equalizer. Considering the best trade-off between complexity and  $Q^2$  factor, the optimum number of filter taps and step size are 30 and 0.0001, respectively.

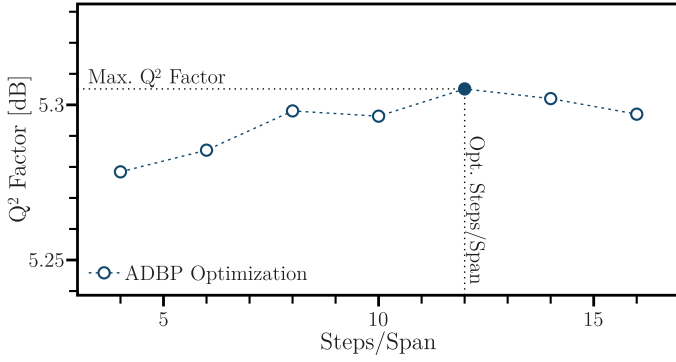


Fig. 4. Optimization of ADBP steps per span.

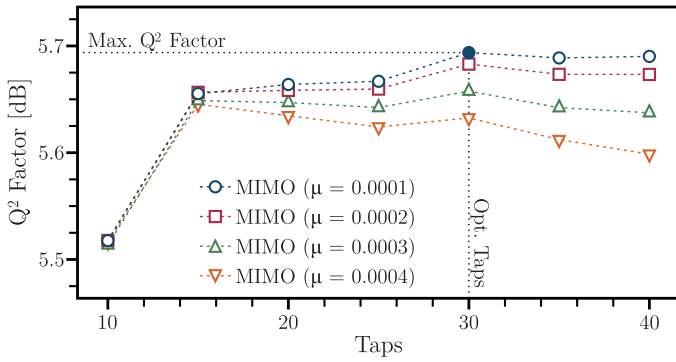
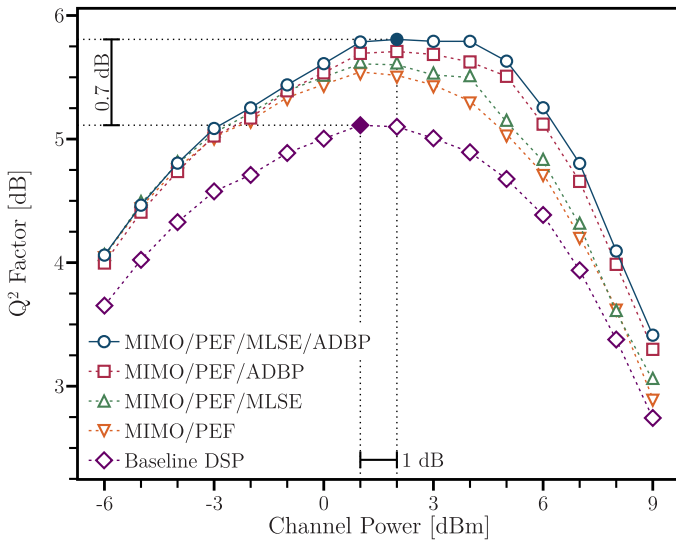


Fig. 5. Optimization of filter taps and step size of 4×4 MIMO equalizer.

Fig. 6.  $Q^2$  versus launch power.

### B. Performance Evaluation

Fig. 6 compares the  $Q^2$  factor as a function of the channel launch power considering the central channel for the baseline and advanced DSP. We evaluate different combinations of the employed DSP blocks, assessing the improvement achieved by each algorithm. The results show that combining the two-stage 4×4 MIMO equalizer with PEF (orange line) increases the

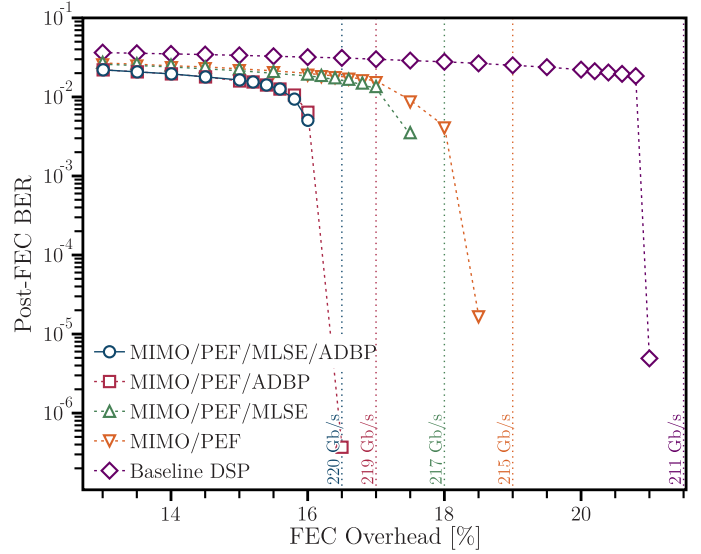


Fig. 7. Post-FEC BER versus FEC overhead.

$Q^2$  factor by 0.4 dB at equivalent launch powers. Adding the MLSE (green line) increases the  $Q^2$  factor by 0.5 dB (0.1 dB improvement) and the optimum channel launch power by up to 1 dB. As the MLSE compensates inter symbol interference (ISI), a slight performance improvement is reached in both linear and nonlinear regimes. If the ADBP algorithm is added to the DSP chain, instead of the MLSE block, the  $Q^2$  gain increases to 0.6 and the optimum launch power increases in the range of 1–2 dB. As expected, the application of ADBP exhibits better performance at high launch powers, where nonlinearities are dominant. The combination of all investigated algorithms on the evaluated DSP stack (blue line) achieves a  $Q^2$  gain improvement equal to 0.7 and a launch power gain in the range of 1–3 dB, respectively. The superior performance is achieved for both linear and nonlinear regimes, demonstrating that the proposed DSP is effective to mitigate both transceiver impairments and fiber nonlinear effects.

Fig. 7 presents the performance of SC-LDPC in terms of post-FEC BER versus FEC overhead, considering the central channel, for the baseline and advanced DSP algorithms, as well as different combinations of DSP blocks. For the baseline DSP (purple line), a FEC overhead of approximately 21.5% is sufficient for error-free operation, resulting in a net data rate of 211 Gb/s. In the case of two-stage 4×4 MIMO equalizer with PEF (orange line), the FEC overhead required to achieve an error-free transmission is 19%, reaching a net data rate of 215 Gb/s. Combining the two-stage 4×4 MIMO equalizer and PEF with only MLSE (green line) and only ADBP (red line), the FEC overhead for error-free operation is equal to 18% and 17%, respectively, resulting in net data rates equal to 217 Gb/s and 219 Gb/s, respectively. Considering all the algorithms (blue line), the FEC overhead required to achieve an error-free operation is 16.5%, resulting in a net data rate of 220 Gb/s.

### C. Complexity Analysis

In previous sections we evaluated the performance gains of selected combinations of DSP algorithms. In this section, the

TABLE I  
DSP ALGORITHMS COMPLEXITY FOR EACH BLOCK

DSP algorithm	Complexity expression (real multiplications per bit)	DSP parameters	Calculated complexity (real multiplications per bit)
CDC [28]	$4 \frac{n[\log_2(n)+1]n_s}{(n-N_{\text{CDC,total}}+1)\log_2(M)}$	$n = 2^{13}$ , $n_s = 2$ , $N_{\text{CDC,total}} = 103$ and $M = 16$	28
PEF [28]	$\frac{4N_1[1+\log_2(N_1)]}{N_1\log_2(M)}$	$N_1 = 2048$ and $M = 16$	12
ADBP [29]	$4N_{\text{span}}N_{\text{sps}} \times$ $\left( \frac{n[\log_2(n)+1]n_s}{(n-N_{\text{ADBP}}+1)\log_2(M)} + n_s \right) +$ $4 \frac{n[\log_2(n)+1]n_s}{(n-N_{\text{CDC,end}}+1)\log_2(M)}$	$N_{\text{span}} = 3$ , $N_{\text{sps}} = 12$ , $n = 2^{13}$ , $n_s = 2$ , $N_{\text{ADBP}} = 47$ , $M = 16$ and $N_{\text{CDC,end}}=56$	1324
MIMO [28]	$\frac{4N_{\text{filters}}N_{\text{taps}}}{\log_2(M)}$	$N_{\text{filters}} = 16$ , $N_{\text{taps}} = 30$ and $M = 16$	480
MLSE [30]	$4(2^m)$	$m = 2$	16
SC-LDPC [31] (baseline DSP)	$\frac{3M_l d_c I_{\text{max}} - 3M_l I_{\text{max}}}{R n_c}$	$M_l = 135000$ , $d_c = 17$ , $R = 0.82$ , $n_c = 50000$ , $W = 15$ and $I_{\text{max}} = 50$	7902
SC-LDPC [31] (MIMO/PEF)	$\frac{3M_l d_c I_{\text{max}} - 3M_l I_{\text{max}}}{R n_c}$	$M_l = 120000$ , $d_c = 19$ , $R = 0.84$ , $n_c = 50000$ , $W = 15$ and $I_{\text{max}} = 50$	7714
SC-LDPC [31] (MIMO/PEF/MLSE)	$\frac{3M_l d_c I_{\text{max}} - 3M_l I_{\text{max}}}{R n_c}$	$M_l = 112500$ , $d_c = 19.65$ , $R = 0.85$ , $n_c = 50000$ , $W = 15$ and $I_{\text{max}} = 50$	7405
SC-LDPC [31] (MIMO/PEF/ADBP)	$\frac{3M_l d_c I_{\text{max}} - 3M_l I_{\text{max}}}{R n_c}$	$M_l = 108750$ , $d_c = 20.34$ , $R = 0.855$ , $n_c = 50000$ , $W = 15$ and $I_{\text{max}} = 50$	7379
SC-LDPC [31] (MIMO/PEF/MLSE/ADBP)	$\frac{3M_l d_c I_{\text{max}} - 3M_l I_{\text{max}}}{R n_c}$	$M_l = 105000$ , $d_c = 21$ , $R = 0.86$ , $n_c = 50000$ , $W = 15$ and $I_{\text{max}} = 50$	7325

computational complexity of the evaluated digital receiver is analyzed. Table I presents the computational complexity in terms of real multiplications per transmitted bit and DSP parameters for each DSP algorithm. The common blocks between the baseline and advanced DSP were omitted in the analysis. The SC-LDPC block is maintained because the varying code rates required for different DSP stacks result in different complexities. We evaluate CDC and ADBP block processing considering  $n$  equal to  $2^{13}$  samples, an oversampling ratio  $n_s$  of 2, and a modulation order  $M$  equal to 16. The CD channel delay spread in number of samples is given by  $N = n_s \tau_D / T$ , where  $\tau_D$  is the dispersive channel impulse response and  $T$  is the symbol duration. Specifically for our CDC implementation, the delay spread corresponding to the entire link,  $N_{\text{CDC,total}}$ , is equal to 103 samples. For the ADBP, we neglect the nonlinear parameter adaptation phase, as it can be sporadically updated and does not significantly contribute to the steady-state complexity. Therefore, the ADBP complexity is calculated as that of the conventional DBP algorithm [29]. As discussed in Section IV-A,

in this work the ADBP considers 12 steps per span ( $N_{\text{sps}}$ ), which are uniformly distributed along the first three fiber spans. In the last two spans the nonlinear stage is turned off and CDC compensation is accounted as a single step. Therefore, the delay spread parameter  $N_{\text{ADBP}}$  used for ADBP in the first three spans is set to 47 samples, and the delay spread parameter  $N_{\text{CDC,end}}$  used for CD compensation in the last two spans is set to 56 samples. Thus, the total complexity of our ADBP stack is equal to the sum of the ADBP complexity for the first three spans ( $N_{\text{span}}=3$  and  $N_{\text{ADBP}}=47$ ), and the CDC complexity for the last two spans ( $N_{\text{CDC,end}}=56$ ). ADBP is carried out with  $N_{\text{sps}}=12$  steps per span.

The PEF considers block processing of  $N_1=2048$  samples. As CDC, the PEF block is based on a static frequency domain equalization (FDE) considering two polarization orientations, requiring the evaluation of four  $N$ -point fast Fourier transforms (FFT) and  $2N$  complex multiplications [28]. The PEF complexity indicated in Table I considers the overlap-save algorithm and a negligible delay spread. The  $4 \times 4$  MIMO is based on the

TABLE II  
 $Q^2$ , LAUNCH POWER AND NET RATE GAINS; TOTAL AND ADDITIONAL COMPLEXITIES; FOR SELECTED DSP STACKS IN RELATION TO THE BASELINE DSP

DSP stack	$Q^2$ gain	Launch power gain	Net data rate gain	Total complexity	Calculated additional complexity
MIMO/PEF	0.4 dB	0 dB	4 Gb/s	8234	304 real mult./bit
MIMO/PEF/MLSE	0.5 dB	0 – 1 dB	6 Gb/s	7941	11 real mult./bit
MIMO/PEF/ADBP	0.6 dB	1 – 2 dB	8 Gb/s	9195	1265 real mult./bit
MIMO/PEF/ADBP/MLSE	0.7 dB	1 – 3 dB	9 Gb/s	9157	1227 real mult./bit

number of complex finite impulse response (FIR) filters  $N_{\text{filters}}$  equal to 16, with 30 taps each, as defined in Section IV-A. The MLSE algorithm considers a memory channel  $m$  equal to 2. Finally, the SC-LDPC complexity is based on the belief propagation (BP) algorithm [32] operating on a Tanner graph constructed from the parity-check matrix [32]. The complexity in terms of real multiplications per iteration depends on the number of rows (check nodes)  $M_l$  and the average degree of check nodes  $d_c$ , as  $3M_l d_c - 3M_l$  [31]. The BP complexity can be generalized for  $I_{\text{max}}$  iterations, as  $3M_l d_c I_{\text{max}} - 3M_l I_{\text{max}}$ . Therefore, the complexity of the BP decoding in terms of multiplications per information bit can be calculated as  $(3M_l d_c I_{\text{max}} - 3M_l I_{\text{max}})/(R n_c)$ , where  $n_c$  is the codeword length. In the case of SC-LDPC decoding, for a sliding window  $W$ ,  $M_l$  is given by  $(n_c - k)W$  [33], where  $k$  is the number of information bits. In the evaluated scenarios, the code rate  $R$  takes the values of 0.82, 0.84, 0.85, 0.855, and 0.86, and the average degree of check nodes  $d_c$  is equal to 17, 19, 19.65, 20.34 and 21 considering the baseline, MIMO/PEF, MIMO/PEF/MLSE, MIMO/PEF/ADBP, and MIMO/PEF/MLSE/ADBP, respectively. The codeword length  $n_c$ , the sliding window  $W$ , and the number of iterations  $I_{\text{max}}$ , are 50000, 15, and 50, respectively.

Table I presents the calculated computational complexity for each DSP algorithm per block. The SC-LDPC decoding exhibits the highest complexity among all investigated techniques, even when compared with the ADBP. This is a consequence of the short reach considered for nonlinear compensation. As expected, the SC-LDPC complexity decreases with the reduction of the FEC overhead. The total complexity for the baseline DSP is equal to 7930 mult./bit. Table II shows the total complexity for each DSP stack. The table also presents  $Q^2$ , launch power, net rate gains, and additional complexity for each DSP stack. The results indicate that the combination of  $4 \times 4$  MIMO and PEF presents a low complexity increase and a 0.4 dB  $Q^2$  gain. Curiously, the application of MLSE with  $4 \times 4$  MIMO and PEF results in a lower increase in complexity and a higher  $Q^2$  gain. This observation can be explained by the fact that the complexity increment caused by the MLSE is compensated by the complexity reduction of the SC-LDPC operating with a higher code rate  $R$ . The reduction in the total complexity obtained by adding the MLSE is also observed when combining it with the ADBP algorithm. The addition of ADBP significantly increases complexity. However, with the application of ADBP, the highest net rate gain is achieved. Compared to previous results without ADBP, the substantial complexity increment using nonlinear compensation can potentially result in higher power consumption by the Rx DSP, mainly if compared to commercial solutions with only

linear impairments mitigation. The previous results support the importance of designing the digital receiver appropriately to compensate transceiver distortions and/or nonlinear effects considering the trade-off between complexity and performance.

## V. CONCLUSION

We evaluated a digital receiver combining advanced DSP algorithms for Tx/Rx impairment compensation, nonlinear mitigation, and variable-rate error correction in unrepeated systems. The bandwidth limitations and IQ skew were compensated using a PEF and a two-stage  $4 \times 4$  MIMO equalizer. Nonlinear compensation was based on a fast convergence ADBP and MLSE. Finally, forward error correction was provided by variable-rate SC-LDPC code. The performance (in terms of  $Q^2$ , launch power and net rate gains) and complexity of the evaluated digital subsystems were experimentally assessed in an unrepeated WDM transmission link with  $17 \times 32$ -GBd DP-16QAM channels over 350-km of large effective area and LL-SMF. We evaluated the computational complexity of linear and nonlinear algorithms using analytic equations. The results indicate that advanced linear and nonlinear algorithms provide modest but incremental gains, suggesting that more substantial benefits can be achieved by combining two or more algorithms. The results also support the need for the selective activation or deactivation of advanced DSP algorithms based on the desired trade-off of complexity and performance.

## ACKNOWLEDGMENT

The authors would like to thank André Souza and Lailson dos Santos for invaluable discussions concerning complexity calculations. The authors would like to thank the anonymous reviewers for important contributions to improve the paper quality.

## REFERENCES

- [1] E. P. da Silva, K. J. Larsen, and D. Zibar, "Impairment mitigation in superchannels with digital backpropagation and MLSD," *Opt. Exp.*, vol. 23, no. 23, pp. 29493–29501, 2015.
- [2] J. H. C. Júnior, T. Sutili, S. M. Rossi, R. C. Figueiredo, and D. A. A. Mello, "Fast adaptive digital back-propagation algorithm for unrepeated optical systems," in *Proc. Opt. Fiber Commun. Conf.*, 2020, pp. 1–3.
- [3] D. A. A. Mello, A. N. Barreto, T. C. de Lima, T. F. Portela, L. Beygi, and J. M. Kahn, "Optical networking with variable-code-rate transceivers," *J. Lightw. Technol.*, vol. 32, no. 2, pp. 257–266, Jan. 2014.
- [4] G.-H. Gho and J. M. Kahn, "Rate-adaptive modulation and low-density parity-check coding for optical fiber transmission systems," *J. Opt. Commun. Netw.*, vol. 4, no. 10, pp. 760–768, 2012.
- [5] E. S. Chou and J. M. Kahn, "Adaptive coding and modulation for robust 50G PONs," in *Proc. Int. Conf. Transp. Opt. Netw.*, 2019, pp. 1–4.

- [6] G.-H. Gho and J. M. Kahn, "Rate-adaptive modulation and coding for optical fiber transmission systems," *J. Lightw. Technol.*, vol. 30, no. 12, pp. 1818–1828, Jun. 2012.
- [7] G.-H. Gho, L. Klak, and J. M. Kahn, "Rate-adaptive coding for optical fiber transmission systems," *J. Lightw. Technol.*, vol. 29, no. 2, pp. 222–233, Jan. 2011.
- [8] R. Rios-Müller *et al.*, "Spectrally-efficient 400-Gb/s single carrier transport over 7200 km," *J. Lightw. Technol.*, vol. 33, no. 7, pp. 1402–1407, Apr. 2015.
- [9] P. Rosa *et al.*, "Unrepeated 64QAM over SMF-28 using Raman amplification and digital backpropagation," in *Proc. Asia Commun. Photon. Conf.*, 2017, pp. 1–3.
- [10] X. Lv *et al.*, "Unrepeated 447Gb/s Nyquist PDM-64QAM transmission over 160 km SSMF with backward Raman amplification," in *Proc. Eur. Conf. Opt. Commun.*, 2015, pp. 1–3.
- [11] J. C. S. S. Januário *et al.*, "Unrepeated transmission of  $10 \times 400\text{G}$  over 370 km via amplification map optimization," *IEEE Photon. Technol. Lett.*, vol. 28, no. 20, pp. 2289–2292, Oct. 2016.
- [12] J. C. Januário *et al.*, "Unrepeated WDM transmission of single-carrier 400G (66-GBd PDM-16QAM) over 403 km," in *Proc. Opt. Fiber Commun. Conf.*, 2017, pp. Th4D.1.
- [13] J. C. Januário *et al.*, "Single-carrier 400G unrepeated WDM transmission over 443.1 km," in *Proc. Eur. Conf. Opt. Commun.*, 2017, pp. 1–3.
- [14] F. Buchali, A. Klekamp, L. Schmalen, and T. Drenski, "Implementation of 64QAM at 42.66 GBaud using 1.5 samples per symbol DAC and demonstration of up to 300 km fiber transmission," in *Proc. Opt. Fiber Commun. Conf.*, 2014, pp. M2A.1.
- [15] F. P. Guiomar *et al.*, "Ultra-long-haul 400G superchannel transmission with multi-carrier nonlinear equalization," in *Proc. Eur. Conf. Opt. Commun.*, 2015, pp. 1–3.
- [16] J. Liang, Y. Fan, Z. Tao, X. Su, and H. Nakashima, "Transceiver imbalances compensation and monitoring by receiver DSP," *J. Lightw. Technol.*, vol. 39, no. 17, pp. 5397–5404, Sep. 2021.
- [17] S.-R. Moon, H.-S. Kang, H. Y. Rha, and J. K. Lee, "C-band PAM-4 signal transmission using soft-output MLSE and LDPC code," *Opt. Exp.*, vol. 27, no. 1, pp. 110–120, 2019.
- [18] T. Yoshida, M. Karlsson, and E. Agrell, "Efficient offline evaluation of FEC codes based on captured data with probabilistic shaping," in *Proc. Opt. Fiber Commun. Conf.*, 2018, pp. M4E.5.
- [19] D. G. M. Mitchell, M. Lentmaier, and D. J. Costello, "Spatially coupled LDPC codes constructed from protographs," *IEEE Trans. Inf. Theory*, vol. 61, no. 9, pp. 4866–4889, Sep. 2015.
- [20] T. Tian and C. R. Jones, "Construction of rate-compatible LDPC codes utilizing information shortening and parity puncturing," *EURASIP J. Wireless Commun. Netw.*, vol. 2005, no. 5, pp. 1–7, 2005.
- [21] F. Buchali, F. Steiner, G. Böcherer, L. Schmalen, P. Schulte, and W. Idler, "Rate adaptation and reach increase by probabilistically shaped 64-QAM: An experimental demonstration," *J. Lightw. Technol.*, vol. 34, no. 7, pp. 1599–1609, 2016.
- [22] S. Iqbal *et al.*, "Probabilistically shaped rate-adaptive polar-coded 256-QAM WDM optical transmission system," *J. Lightw. Technol.*, vol. 38, no. 7, pp. 1800–1808, 2020.
- [23] P. N. Goki and L. Poti, "Rate loss reduction through look-up table design for hierarchical distribution matcher in probabilistic amplitude shaped systems," in *Proc. Eur. Conf. Opt. Commun.*, 2021, pp. 1–4.
- [24] S. Dris, S. Alreesh, and A. Richter, "Blind polarization demultiplexing and equalization of probabilistically shaped QAM," in *Proc. Opt. Fiber Commun. Conf.*, 2019, pp. W1D.2.
- [25] F. A. Barbosa, S. M. Rossi, and D. A. A. Mello, "Clock recovery limitations in probabilistically shaped transmission," in *Proc. Opt. Fiber Commun. Conf.*, 2020, pp. M4J.4.
- [26] F. A. Barbosa, S. M. Rossi, and D. A. A. Mello, "Phase and frequency recovery algorithms for probabilistically shaped transmission," *J. Lightw. Technol.*, vol. 38, no. 7, pp. 1827–1835, Apr. 2020.
- [27] J. H. da Cruz Júnior, F. Della Lucia, T. Sutili, D. A. de Arruda Mello, and R. C. Figueiredo, "Gradient-based optimization for unrepeated optical systems," in *Proc. Int. Microw. Optoelectron. Conf.*, 2019, pp. 1–3.
- [28] B. Spinnler, "Equalizer design and complexity for digital coherent receivers," *IEEE J. Sel. Topics Quantum Electron.*, vol. 16, no. 5, pp. 1180–1192, Sep./Oct. 2010.
- [29] O. Sidelnikov, A. Redyuk, and S. Sygletos, "Equalization performance and complexity analysis of dynamic deep neural networks in long haul transmission systems," *Opt. Exp.*, vol. 26, no. 25, pp. 32765–32776, 2018.
- [30] Z. Qin and K. C. Teh, "Reduced-complexity turbo equalization for coded intersymbol interference channels based on local search algorithms," *IEEE Trans. Veh. Technol.*, vol. 57, no. 1, pp. 630–635, Jan. 2008.
- [31] Y. Wang, H. Yin, Z. Yang, and Y. Huang, "An improved belief propagation algorithm based on exponential model," in *Proc. Int. Conf. Signal Process.*, 2018, pp. 702–705.
- [32] T.-C. Chen, C.-J. Li, and E.-H. Lu, "A hybrid belief propagation decoding algorithms of LDPC codes for fast convergence," in *Proc. Cross Strait Quad-Regional Radio Sci. Wireless Technol. Conf.*, 2013, pp. 389–392.
- [33] A. R. Iyengar, M. Papaleo, P. H. Siegel, J. K. Wolf, A. Vanelli-Coralli, and G. E. Corazza, "Windowed decoding of protograph-based LDPC convolutional codes over erasure channels," *IEEE Trans. Inf. Theory*, vol. 58, no. 4, pp. 2303–2320, Apr. 2012.